



Queensland University of Technology
Brisbane Australia

This is the author's version of a work that was submitted/accepted for publication in the following source:

[Hoshyargar, Faegheh, Crawford, Jessica, & O'Mullane, Anthony P.](#)
(2017)
Galvanic replacement of the liquid metal galinstan.
Journal of the American Chemical Society, 139(4), pp. 1464-1471.

This file was downloaded from: <https://eprints.qut.edu.au/99827/>

© Copyright 2016 American Chemical Society

This document is the Accepted Manuscript version of a Published Work that appeared in final form in

Journal of the American Chemical Society, copyright © American Chemical Society after peer review and technical editing by the publisher. To access the final edited and published work see <https://doi.org/10.1021/jacs.6b05957>

Notice: *Changes introduced as a result of publishing processes such as copy-editing and formatting may not be reflected in this document. For a definitive version of this work, please refer to the published source:*

<https://doi.org/10.1021/jacs.6b05957>

Galvanic Replacement of the Liquid Metal Galinstan

Faegheh Hoshyargar,[†] Jessica Crawford,[†] Anthony P. O'Mullane^{*,†}

[†]School of Chemistry, Physics and Mechanical Engineering, Queensland University of Technology (QUT), Brisbane, QLD 4001, Australia

KEYWORDS: liquid metal, galvanic replacement, nanoparticles, black gold, methylene blue degradation

ABSTRACT: The galvanic replacement reaction is a highly versatile approach for the creation of a variety of nanostructured materials. However, the majority of reports are limited to the replacement of metallic nanoparticles or metal surfaces. Here we extend this elegant approach and describe the galvanic replacement of the liquid metal alloy galinstan with Ag and Au. This is achieved at a macrosized droplet to create a liquid metal marble that comprises a liquid metal core and a solid metal shell whereby the morphology of the outer shell is determined by the concentration of metallic ions used in the solution during the galvanic replacement process. In principle, this allows one to recover precious metal ions from solution in their metallic form which is immobilized on the liquid metal and therefore easy to recover. The reaction is also undertaken at liquid metal microdroplets created via sonication to produce Ag and Au based galinstan nanorice particles. These materials are characterized with SEM, XRD, TEM, SAED, EDX, XPS, UV-visible spectroscopy and open circuit potential versus time experiments to understand the galvanic replacement process. Finally, the nanosized materials were investigated for their catalytic activity towards the reduction of methylene blue in the presence of sodium borohydride. This approach illustrates a new avenue of research for the galvanic replacement process and in principle could be applied to many more systems.

INTRODUCTION

Galvanic replacement involving nanoscale objects has been the subject of intensive research since 2002 when it was first reported by Xia and colleagues.¹ Since then, several comprehensive review articles have been written on the subject either directly or as part of a broader review of hollow and porous materials.²⁻¹⁰ Although the electrochemical principle behind this reaction is considerably older, Xia was the first to demonstrate the phenomenon on the nanoscale where Au hollow nanostructures were created from Ag nanoparticles.¹ The electrochemical reaction is straightforward in that a sacrificial template such as Ag is oxidised in the presence of ions of a different metal such as Au³⁺ which have a higher reduction potential which are subsequently reduced to the metallic state at the template surface. Under appropriate reaction conditions a variety of nanostructured materials can be formed such as hollow nanoparticles of different shapes, sizes and composition. This can be extended further by combination with a co-reduction reaction whereby a reductant can be introduced to create bimetallic or alloyed hollow nanostructures or layered nanomaterials.² With regards to the galvanic replacement of metallic nanoparticles and macroscopic surfaces the field is very mature and the resultant materials have been used in numerous electro-(catalytic), plasmonic and biomedical imaging applications.¹¹⁻¹⁸

There have also been reports to extend the concept of galvanic replacement to systems other than pure metals. Oh et al have demonstrated that Mn₃O₄ nanocrystals could be galvanically replaced using iron perchlorate to produce hollow

nanocrystals of Mn₃O₄/γ-Fe₂O₃ which ultimately converted into cagelike γ-Fe₂O₃ nanomaterials.¹⁹ These were utilised as anode materials in Li ion batteries. Metal oxides such as Cu₂O have also been galvanically replaced in solutions of appropriate pH to create Cu₂O/Pd and Cu₂O/Au nanocomposites.²⁰ Other reports have included the galvanic replacement of semiconducting organic charge transfer complexes such as MTCNQ (TCNQ = tetracyanoquinodimethane) and MTCNQF₄ (TCNQF₄ = 2,3,5,6-tetrafluoro-7,7,8,8-tetracyanoquinodimethane) with Au, Ag, Pt and Pd nanomaterials for (photo)-catalytic applications.²¹⁻²⁴

Therefore, it is clear that the process of galvanic replacement is attractive because excellent control can be achieved on the nanoscale which can be tuned for the application of interest. However to date there has not been an attempt to explore the galvanic replacement of a liquid metal such as galinstan which is a room temperature liquid metal alloy of 68.5% Gallium, 21.5% Indium and 10.0% Tin. It is apparent that the individual metal components can be readily oxidised when the electrochemical series is considered and oxidants such as Ag⁺ and Au³⁺ ions should facilitate the galvanic replacement process. It is noteworthy that liquid metals in their own right, have received significant attention recently in diverse areas such as plasmonics,^{25,26} liquid metal enabled pumps,²⁷ actuators,²⁸ as a coolant,²⁹ electronics,^{30,31} fluidic antennas,³² wearable sensors,^{33,34} repairable circuitry,³⁵ microfluidics³⁶ and also when modified into liquid metal marbles which consist of a coating of semiconducting nanomaterials on the liquid metal core.³⁷ The latter has been used in photocatalytic applications, electrochemical heavy metal ion sensing and

in actuator applications.³⁷⁻³⁹ Therefore the ability to manipulate the chemistry of liquid metals in a facile manner may have significant implications for many applications as well as being a system of fundamental interest.

Therefore, in this work we explore the galvanic replacement of liquid metal galinstan with Ag and Au on both the bulk scale to generate liquid metal core/solid metal shell marbles and nanorice particles on the nanoscale. We explore the latter as heterogeneous catalysts for the degradation of the dye methylene blue in the presence of sodium borohydride. We believe this approach opens up a new avenue of research in the important area of galvanic replacement.

EXPERIMENTAL SECTION

Materials and Chemicals. Potassium tetrabromoaurate(III) hydrate ($\text{KAuBr}_4 \cdot x\text{H}_2\text{O}$, 99.9%), Potassium gold(III) chloride (KAuCl_4 , 99.995%), polyvinylpyrrolidone (PVP, average molar weight = 10,000) and sodium borohydride (NaBH_4 , 99.99%) were purchased from Sigma-Aldrich. Methylene blue (MB) was obtained from EMD Chemicals and silver nitrate (AgNO_3 , 95%) from Australian Chemical Reagents. Galinstan (Galinstan fluid 4N) was purchased from Geratherm Medical AG.

Galvanic replacement process. In the initial experiments a galinstan droplet was placed in aqueous solutions of AgNO_3 or KAuBr_4 of different concentrations ranging from 0.1 to 5 mM or in 0.1 and 1 mM aqueous solution of KAuCl_4 for 72 h. For the galvanic replacement of micro-sized galinstan a liquid droplet was sonicated in an aqueous solution of either AgNO_3 or KAuBr_4 . The Ag-GalInSn material was prepared by sonicating 80 mg galinstan in 4.9 ml aqueous solution of 5 mM AgNO_3 for 30 min followed by adding 0.1 ml aqueous solution of 5 mg/ml PVP to the solution. The Au-GalInSn material was prepared by sonicating 200 mg galinstan in 5 ml aqueous solution of 1 mM $\text{KAuBr}_4 \cdot x\text{H}_2\text{O}$ for 30 min. All aqueous solutions were prepared from water (resistivity of 18.2 $\text{M}\Omega \cdot \text{cm}$ at 25°C) purified by use of a Milli-Q reagent deionizer (Millipore). Sonication was carried out in a sonication bath (Soniclean Pty. Ltd. Soniclean 750HT, 220/240V AC, 50/60Hz, 380W).

Material Characterization. Material characterization was carried out using field emission scanning electron microscopy (FESEM, Zeiss Sigma VP field emission scanning electron microscope equipped with an Oxford XMax 50 Silicon Drift energy dispersive X-ray detector at 20 kV under high-vacuum), high resolution transmission electron microscopy and selected area electron diffraction (HRTEM and SAED, JEOL 2100 200 kV transmission electron microscope equipped with high-sensitivity silicon drift X-ray detector (Oxford XMax) for compositional analysis, with an Ultra-high-resolution pole piece, Gatan Orius SC1000 CCD camera and LaB_6 gun), X-ray photoelectron spectroscopy (XPS, Omicron MultiProbe system using a non-monochromated Al K α X-ray source) and UV-visible spectroscopy (Agilent Cary® 60 UV-Visible spectrophotometers). Colloidal nanocomposites were drop casted onto cleaned Si wafers and amorphous carbon coated copper grids for SEM and TEM studies, respectively, and immobilized by solvent evaporation. SEM samples of the large droplets of galinstan modified with silver or gold

were prepared by collecting the skin formed on the galinstan droplet, dispersing in deionized water and drop casting onto cleaned Si wafers. A colloidal solution of Ag-GalInSn was diluted 5 times to prepare samples for SEM, TEM and UV-vis absorption studies. The XPS data were analyzed using CasaXPS software version 2.3.16. Two dimensional (2D) X-ray diffraction (XRD) patterns were acquired with a Rigaku SmartLab using a copper (Cu) target (40 kV, 40 mA) and a Hypix 3000 detector (vertical orientation). A parallel beam was generated by the cross beam optics unit and then further conditioned to a smaller area using a CBO-*f* unit and 0.5 mm height limiting slit. The samples were placed on a stage that allows for movement in the X and Y directions. A flat part of the sample was chosen for analysis, then 2D exposures (10 s) were collected across the 15 – 90 °2 θ range. The exposures were then integrated to 0/1D profiles using Rigaku 2D Data Processing Software (2DP).

Electrochemical Experiment. A hanging galinstan drop electrode (HGDE) was used as the working electrode.³⁷ The reference electrode was Ag/AgCl (aqueous 3 M KCl) and platinum was used as the counter electrode. The electrochemical experiment was carried out using a Biologic VSP-300 potentiostat. A galinstan droplet suspended from a syringe was allowed to make contact with water immediately before running the open circuit potential (OCP) versus time experiment. The required volume of AgNO_3 aqueous solution was injected into the cell to give a final concentration of 5 mM.

Catalytic Reaction. 0.1 ml of the catalyst (either colloidal Ag-GalInSn or Au-GalInSn) was injected into the reaction mixture with a total volume of 3 ml (containing 7.2×10^{-5} M methylene blue and 1.2×10^{-2} M sodium borohydride) in a quartz cuvette at (25 ± 2) °C and the catalytic activity was monitored by UV-vis spectroscopy using an Agilent Cary® 60 UV-Visible spectrophotometer. For the control experiment, 80 mg galinstan was sonicated in 5 ml deionized water (DIW) for 30 min and used as the catalyst following the same procedure described for Ag-GalInSn and Au-GalInSn.

RESULTS AND DISCUSSION

Initial investigations were undertaken with a galinstan droplet placed in an aqueous solution of AgNO_3 . The liquid metal droplets were exposed to 0.1, 0.5, 1 and 5 mM AgNO_3 aqueous solutions and the changes in the appearance of the droplet were monitored and recorded at 24 h intervals up to 72 h. Figure 1 shows digital images which illustrate the significant changes in the appearance and morphology of the droplet as a function of concentration and time. Upon initial contact ($t = 0$) with the AgNO_3 solution, the shiny metallic galinstan droplets turned a grey colour almost immediately, in particular in the case of higher concentrations whereas the droplet in 0.1 mM remained pristine. However, after 24 h a grey coloured skin formed on the galinstan droplet at the lowest concentration of 0.1 mM (Figure 1b). Interestingly, at $t = 24$ h, the galinstan droplet in the 5 mM AgNO_3 solution grew much larger than the originally sized droplet and turned black. The colour of the outer coating did not change from $t = 24$ h to $t = 48$ h while its thickness increased (Figure 1c and 1d). The outer black layers were allowed to develop for 72 h and were subsequently collected and subjected to further characterization by FESEM/EDX.

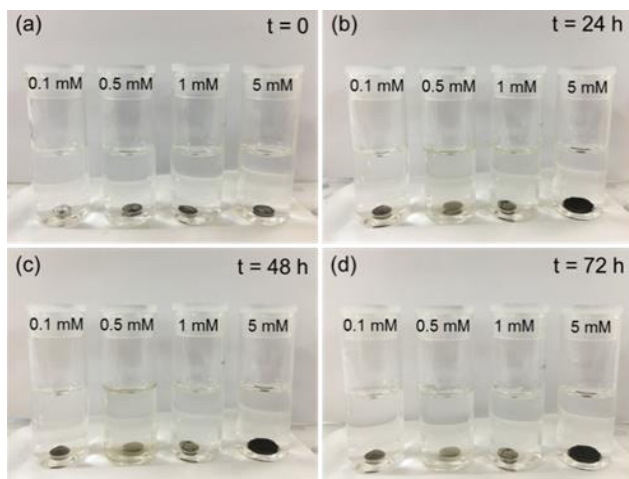
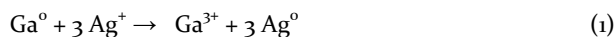


Figure 1. Formation of black silver in AgNO_3 solutions of varied concentrations after (a) 0, (b) 24, (c) 48 and (d) 72 h.

Figure 2a and 2b show the FESEM images of the skin created in 0.1 mM solution after 72 h. At this very low concentration, the outer skin that is formed is very thin and consists of structures that are consistent with oxidised galinstan, i.e. wrinkled microstructures that are indicative of Ga_2O_3 .³⁸ There is some evidence of small spherical shaped particles (Figure 2b) attributed to the formation of metallic silver (EDX analysis shows a 2.9% Ag content, Table S1). The morphology of the outer skin changed considerably at the higher AgNO_3 concentrations of 0.5 mM (Figures 2c and 2d) and 1 mM (Figures 2e and 2f). Here more block like crystals were formed and the Ag content increased to 10.7% and 11.2%, respectively (Table S1). The outer skin obtained from the 5 mM AgNO_3 solution also showed a marked difference in morphology from the other samples and is composed of micrometer sized multipods which grow all over the skin. These multipods are geometrically asymmetric and the branches grow in random directions as shown in Figures 2g and 2h. The silver content in this case was significant and increased to 51.4% (Table S1).

Given the observations seen here and the formation of metallic Ag on the surface of the galinstan drop it indicates that a galvanic replacement process is occurring. In principle, galvanic replacement takes place at the liquid metal-solution interface, namely, the galinstan droplet's surface which serves as the sacrificial template for the growth of the obtained nanostructures. When the standard reduction potentials of $\text{Ga}^{3+}/\text{Ga}^0$, $\text{In}^{3+}/\text{In}^0$, $\text{Sn}^{2+}/\text{Sn}^0$ and Ag^+/Ag^0 which are -0.529, -0.340, -0.138 and 0.799 V vs. SHE,⁴⁰ respectively, are considered it indicates that there are significant thermodynamic driving forces for such a replacement reaction to take place. This will occur in an analogous manner to that seen for the many reports in the literature that describe this phenomenon. The major difference in this case is that the template is a liquid rather than a solid nanoparticle or surface as reported previously. For the case of galinstan, in principle all three components of the liquid can be replaced when in contact with AgNO_3 with the highest driving force being for the replacement of Ga, which has the lowest standard reduction potential. This is reflected in the EDX data where the consumption of Ga is the most rapid when increasing the AgNO_3

concentration (Table S1). This redox reaction between Ga and Ag^+ ions can be represented by equation 1.



Upon liberation of Ga^{3+} ions they will immediately react with dissolved O_2 to form Ga_2O_3 which accounts for the large concentration of oxygen found in the EDX analysis. Therefore, the outer skin of galvanically replaced galinstan consists of Ga_2O_3 and metallic Ag and minor components of In and Sn.

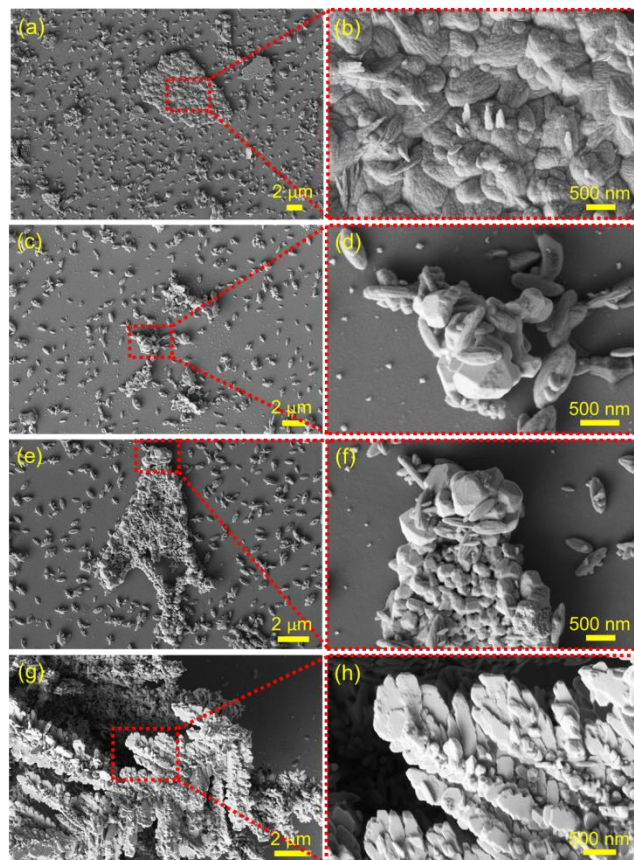


Figure 2. FESEM images of black silver formed on a galinstan droplet in (a,b) 0.1, (c,d) 0.5, (e,f) 1 and (g,h) 5 mM AgNO_3 aqueous solution.

In order to study whether the galvanic replacement of galinstan is possible with other metals, this experiment was also carried out using a gold salt. In this case, galinstan droplets were placed into aqueous solutions of KAuBr_4 and on this occasion changes in the colour of the solution could be monitored as well as in the appearance of the liquid droplet. Similar to the silver case, a black skin was readily formed on galinstan at the initial point ($t = 0$) in the case of the 5 mM gold salt solution; however this was not the case for solutions with lower concentrations (Figure 3a). As observed in Figure 3b, the development of a black skin on galinstan droplets in the lower concentration solutions was only initiated after 24 h. Again as the template, the galinstan's surface is where the black skin grows after the galvanic replacement of Ga/Sn/In elements with AuBr_4^- ions. There is also a significant driving force for this reaction to occur when the standard reduction

potential of the $\text{AuBr}_4^-/\text{Au}^0$ couple of 0.85 V vs. SHE is considered.

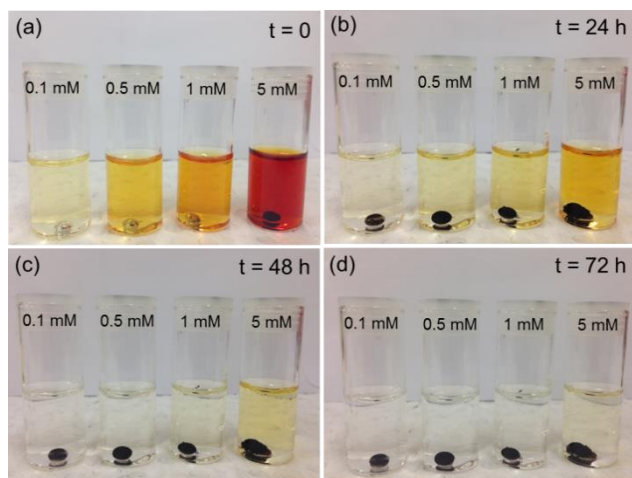
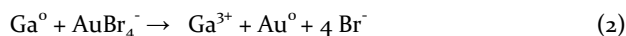


Figure 3. Formation of black gold on galinstan in KAuBr_4 aqueous solutions of varied concentrations after (a) 0, (b) 24, (c) 48 and (d) 72 h.

From the EDX analysis (Table S2) the major reactant is Ga and the reaction can be presented as,



Figures 3c and 3d indicate that the growth of this black skin continues with time and that the thickness of the outer skin increases until all the AuBr_4^- ions in the solution are consumed (the solution becomes colorless). As can be seen from the images, compared to the fresh droplet, the galinstan becomes highly elongated with time, which is assumed to be due to the extra weight of material that is being added by the developing skin (best observed in the 5 mM solution as the skin is thicker and therefore heavier). After 72 h, the outer skins were subjected to further investigations by a combined FESEM/EDX analysis.

As illustrated in Figures 4a and 4b, at the lowest concentration of 0.1 mM, the growth of gold is limited (0.6% Au, see Table S2). However even at this low concentration well-defined hierarchical nanostructures are formed which are composed of multipod assemblies of Au nanoparticles which is significantly different to the silver case where spherical particles were formed (Figure 2b). The formation of dendritic materials in the case of gold can be attributed to the liberation of Br^- ions into solution (eq. 2) where it is known from electrochemical studies that the presence of halides can promote the formation of anisotropic structures.^{41,42} It is also known that Br^- ions interact strongly with specific crystal facets of gold which would perturb the growth process.⁴³ Interestingly, when the KAuBr_4 solution was replaced with a KAuCl_4 solution, elongated dendrites were not formed as shown in Figure S1a and b for 0.1 mM and in Figure S1c and d for 1 mM solution, confirming a strong interaction of the liberated bromide ions with the growing gold deposit rather than with chloride ions. At 0.5 mM, hierarchical structures were also formed but with fewer branches (Figures 4c and

4d) and the Au contribution increases quite substantially to 21.8% (Table S2). Figures 4e and 4f show the morphology of the nanostructures obtained in a 1 mM KAuBr_4 solution where branch formation becomes even more inhibited and the Au content increases to 47.3% (Table S2). At 5 mM KAuBr_4 (Figures 4g and 4h), no branched structures are formed, instead, large block like crystals which are coalesced are evident. The gold content under these conditions increases to 55.6 %, (Table S2). At the higher KAuBr_4 concentrations the rate of reduction is significantly faster and therefore the formation of branched dendritic like structures is suppressed, even in the presence of bromide ions. The formation of the dendrites is generally favoured by slower growth conditions in dilute solutions where the diffusion limited aggregation growth model operates.⁴⁴ Under the conditions of high concentration, the growth process is too rapid to allow this to occur or be influenced by the presence of growth directing halide ions and therefore denser and less open structures are formed. XRD experiments confirm that the silver and gold outer shells formed via galvanic replacement of galinstan in low and high concentration metal salt solutions are polycrystalline with a face centred cubic crystal structure (Figure 5). This was also confirmed by SAED experiments (Figure 5 f and h), which show the polycrystalline nature of both the Ag and Au samples. There are also no peaks present for Ga_2O_3 indicating that the surface oxide is amorphous.

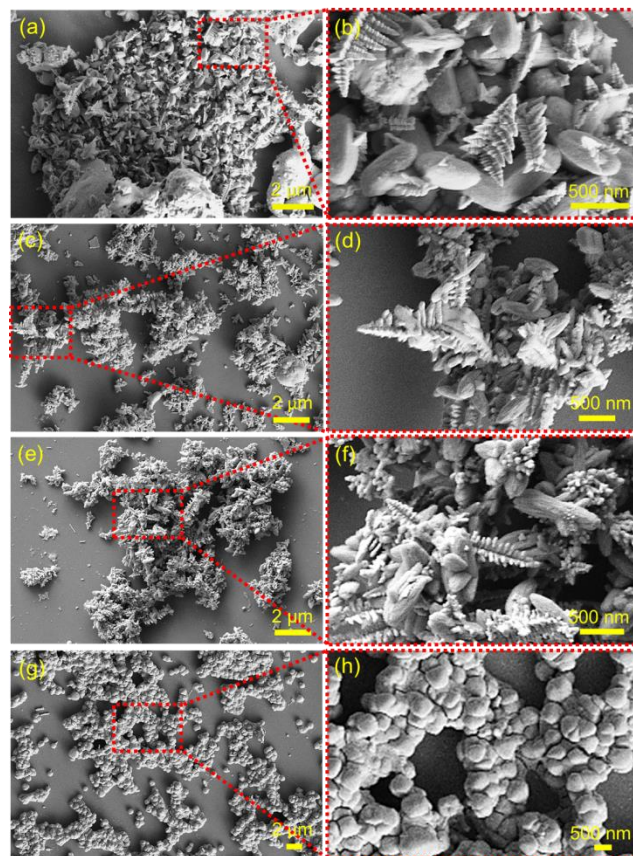


Figure 4. FESEM images of black gold formed on a galinstan droplet in (a,b) 0.1, (c,d) 0.5, (e,f) 1 and (g,h) 5 mM KAuBr_4 aqueous solution.

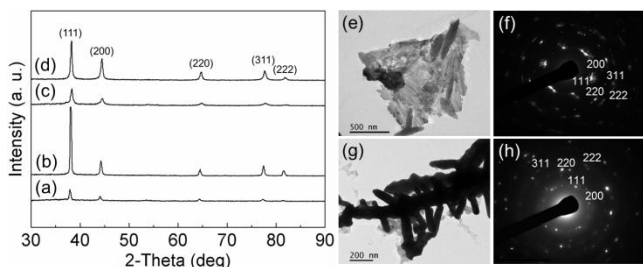


Figure 5. XRD patterns of black silver and black gold formed on a galinstan droplet in (a) 0.5, (b) 5 mM AgNO_3 and (c) 0.5, (d) 5 mM KAuBr_4 aqueous solutions, TEM and SAED pattern of black silver and black gold formed on galinstan droplet in (e, f) 5 mM AgNO_3 and (g, h) 5 mM KAuBr_4 aqueous solutions.

As previously mentioned, the galvanic replacement reaction takes place at the galinstan-solution interface. At the concentration of metal salts used here, complete consumption of the liquid metal is unlikely to occur and the metal salts are the limiting reagents, as evidenced by the almost complete disappearance of the characteristic red/orange colour of KAuBr_4 after 72 h. To illustrate this, the galvanically replaced liquid metal drop was removed from the solution and cut with a scalpel blade which shows the shiny unreacted liquid metal core as well as the outer skin (Figure 6 and video S1). This confirms under these conditions that a liquid metal marble is formed that consists of a solid metal shell encapsulating a liquid metal core. EDX analysis of the core of this marble indicates that its composition is unchanged from the starting material (Figure S2).

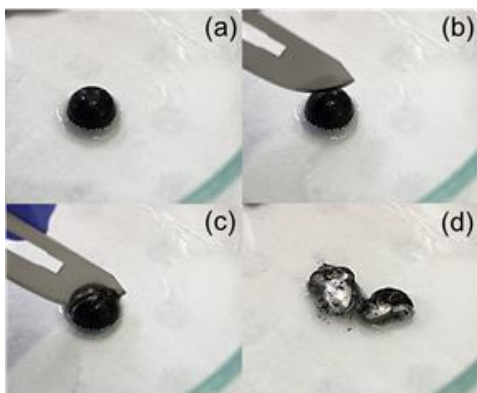


Figure 6. Successive snapshots of cutting through the black gold skin exposing unreacted galinstan in the core.

This system is quite different to previous studies on liquid metal marbles³⁷ where liquid galinstan was modified with powders of semiconducting material such as WO_3 and this approach may open up a new avenue of research into these interesting liquid metal marble systems. It also indicates a possible route for the recovery of precious metals that are in their ionic form. In principle, any metal ion that has a standard reduction potential higher than that of $\text{Ga}^0/\text{Ga}^{3+}$ could be recovered in an aqueous solution. We also investigated the reduction of Pd^{2+} , Pt^{2+} and Cu^{2+} ions and found that metal shells are also created on the galinstan droplet in each case. For the case of copper the reaction was found to be much slower than all other systems (1 week to form a non-continuous film on a galinstan drop) and can be related to the less positive standard reduction potential of the $\text{Cu}^{2+}/\text{Cu}^0$

(0.340 V vs SHE) couple compared to that of the Ag, Au, Pt and Pd systems. This indicates that the major driving force is likely to be thermodynamic in nature and not dictated by the number of electrons involved in the replacement process.

From previous studies on liquid metal gallium-indium⁴⁵ and galinstan it was found that sonicating liquid metals in solution resulted in the formation of liquid metal micro/nanodroplets that improved the performance in particular for galinstan in applications such as heavy metal ion sensing,³⁸ gas sensing,⁴⁶ photocatalysis³⁹ and heterogeneous catalysis.⁴⁷ Therefore the galvanic replacement of galinstan was also studied under sonication conditions. For this experiment a galinstan droplet was sonicated in 5 mM AgNO_3 aqueous solution for 30 min. Under sonication the liquid metal breaks apart into smaller particles which in principle should increase the reactivity towards silver ions due to a simple increase in surface area of the liquid metal. It was found that the solution turned yellow only a few seconds after sonication, which is highly indicative of the formation of Ag nanostructured materials. The reaction was carried out for 30 min after which 0.1 ml polyvinylpyrrolidone (PVP) aqueous solution (5 mg/ml), a known nanoparticle capping agent,⁴⁸ was added to the solution to maintain the stability of obtained nanocomposite in colloidal form (final concentration of PVP was 0.1 mg/ml). When PVP was not added, the particles agglomerated while the addition of the stabilizing agent increased the lifetime of the colloidal suspension up to 7 days. The material formed with this approach is denoted as Ag-GaInSn.

Figure 7a shows an overview FESEM image of the as-synthesized Ag-GaInSn. As observed in figure 7b, the product is composed of monodispersed nanorice-like particles with dimensions of on average $500 \text{ nm} \times 150 \text{ nm}$. A high resolution TEM image is shown in Figure 7c. The nanorice particles are in fact composed of smaller particles assembled to form ellipsoid grains (Figure 7d). EDX analysis of Ag-GaInSn nanocomposite (Table S3, supporting information) revealed a contribution of 4.5% silver in the nanocomposite (sample diluted 5 times).

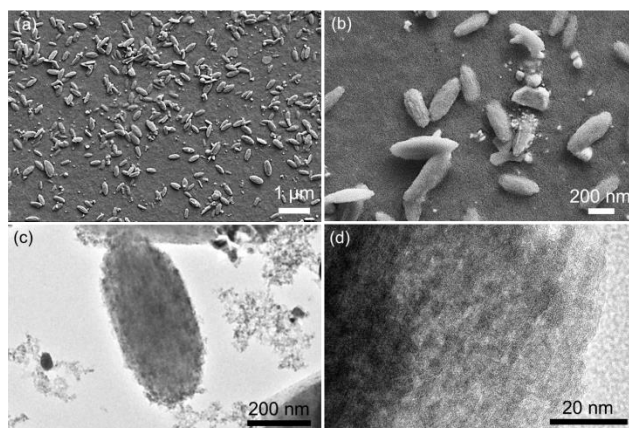


Figure 7. FESEM and TEM images of Ag-GaInSn nanocomposite. (a) Overview and (b) magnified FESEM image, (c) correspondent TEM image and (d) high resolution image of an individual nanorice particle.

The formation of metallic Ag nanoparticles was also confirmed by the appearance of a characteristic surface plasmon resonance band at 438 nm as monitored by UV-vis spectroscopy (Figure 8a). Some distinct spherical particles can also be observed in the SEM images in Figure 7a and b that are not part of the nanorice particles which are responsible for the observation of the well-defined surface plasmon resonance peak at 438 nm. The broad absorption from 450 to 700 nm could be attributed to the nanorice particles. The hypothesis that Ag nanoparticles are formed as a result of galvanic replacement reaction was also confirmed electrochemically. A hanging galinstan drop electrode (HGDE) electrode was immersed into a 5 mM AgNO_3 solution and an open circuit potential (OCP) *versus* time experiment was carried out (Figure 8b). The experiment was run for 30 min for consistency with the sonication time. The experiment was carried out by injecting AgNO_3 into water where the HGDE was already in position to capture the first contact of galinstan with Ag^+ ions. The rapid rise of potential from -0.39 to 0.46 V within the first 160 s indicates that galinstan rapidly oxidizes in the presence of Ag^+ ions. After 160 s, the potential continues to increase but at a very slow rate and does not reach the expected value for an Ag electrode in 5 mM AgNO_3 of 0.663 V vs SHE. This is due to the surface not being entirely composed of silver as there is also Ga_2O_3 present as well as the consumption of Ag^+ ions which will affect the potential of the electrode. After the experiment it can be seen from the inset in Figure 8b that the part of the HGDE that was immersed into the electrolyte is covered with the black silver skin as seen in Figure 1.

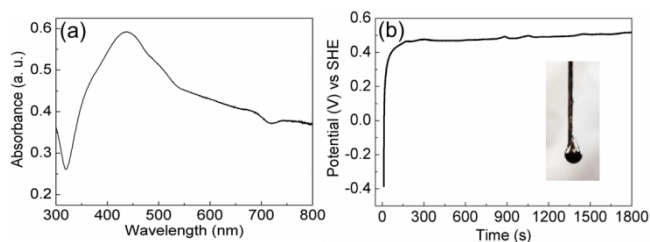


Figure 8. (a) UV-vis spectrum of Ag-GaInSn nanocomposite solution and (b) OCP vs. time recorded in 5 mM AgNO_3 solution with HGDE as a working electrode (inset: HGDE half-submerged in the electrolyte solution in OCP experiment).

The galvanic replacement of galinstan with gold was also studied using the sonication approach. When galinstan was sonicated in a 1 mM aqueous solution of KAuBr_4 for 30 min a pink colour formed which is highly indicative of gold nanoparticle formation. The as-obtained particles were then investigated by FESEM and HRTEM (Figure 9). Nanorice particles were also observed which are quite similar to those formed when AgNO_3 was used (Figure 7), however they are slightly larger (600 nm \times 250 nm). Similar to the Ag analogue, the nanorice particles appear to be porous and made up of smaller particles (Figure 9d). EDX analysis (Table S3, supporting information) revealed a 5.2% contribution of Au nanoparticles.

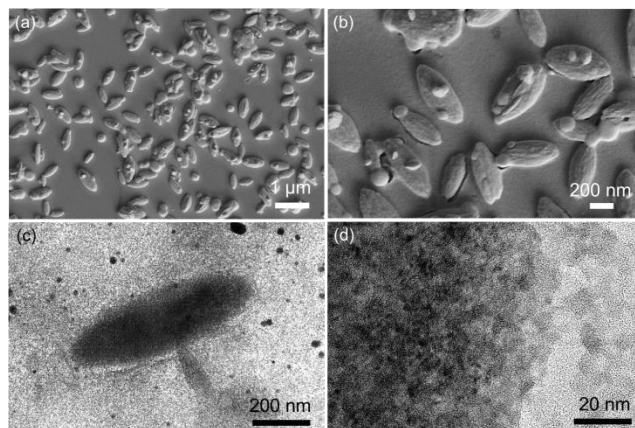


Figure 9. FESEM and TEM images of Au-GaInSn nanocomposite. (a) Overview and (b) magnified FESEM image, (c) correspondent TEM and (d) high resolution image of an individual nanorice particle.

EDX mapping (Figure 10) and an EDX profile (Figure S3) clearly show the presence of Ga, In, Sn, Au and O elements. However, the In content in the nanorice particles is particularly depleted when compared to starting galinstan (which could be observed from the In line in Figure S3). This is most likely due to the formation of the stable KInBr_3 species during the course of the galvanic replacement of metallic In with gold ions (Figure S4). From the EDX mapping data it is apparent that there is some gold contained within the nanorice particles but there is a significant amount of gold that surrounds the nanorice particles but which also is present as isolated nanoparticles (Figure 10).

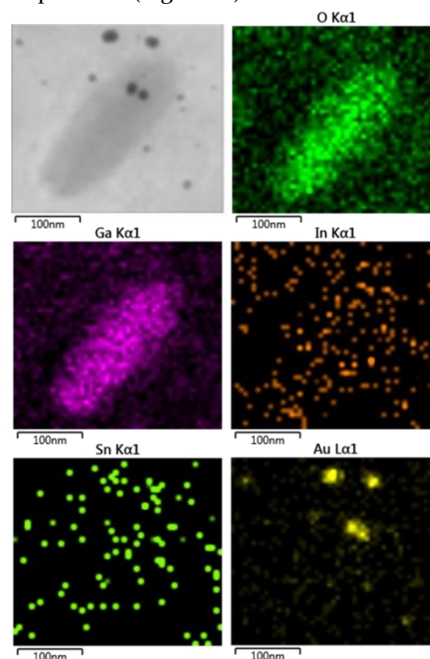


Figure 10. EDX mapping of Au-GaInSn nanocomposite obtained in 1 mM KAuBr_4 aqueous solution.

It is not surprising that isolated nanoparticles of both Ag and Au are formed with this approach as under sonication conditions any metallic nanoparticle that is formed under these forces could detach from the liquid metal. For the large droplet (Figures 1 and 3) the reaction occurs under quiescent conditions and therefore Ag and Au can nucleate and grow into solution and not detach from the liquid droplet. It is notable that the colloidal nanocomposite was stable in the solution even after 30 days without the need for a stabilizing agent even when KAuBr_4 solution was added to galinstan after it had been previously sonicated (Figure S5). The formation of metallic gold is also readily observed by the appearance of a surface plasmon resonance band at 533 nm (Figure 11) and is due to the isolated Au nanoparticles formed during the reaction as seen in the TEM image in Figure 10.

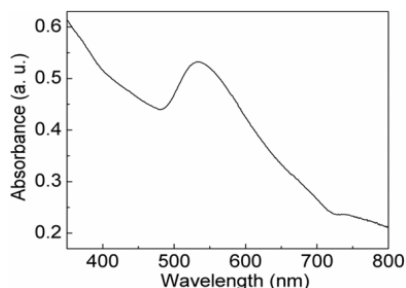


Figure 11. UV-vis spectrum of Au-GaInSn nanocomposite solution.

The surface composition of the Au-GaInSn was investigated in more detail using XPS. The Ga 3d core level spectrum (Figure 12a) with a peak at 20.3 eV is consists of 3 components at 20.4, 18.6 and 15.9 eV, the latter being an overlapping In 4d (metallic indium) peak.³⁸ The In 3d core level spectrum shows two distinctive peaks at 445.3 and 452.9 eV (Figure 12b). These peaks are consistent of one major and one minor component as shown in Figure 12b. The minor components at 443.2 (In $3d_{5/2}$) and 450.8 eV (In $3d_{3/2}$) are essentially contributed by In^0 whereas the major components at 445.4 and 452.9 eV reveal the formation of indium oxide (In_2O_3).³⁸ The Sn 3d spectrum (Figure 12c) with main peaks at 486.7 and 492.1 eV shows a comparable contribution of metallic tin and tin oxide (Sn^{4+}) on the surface.³⁸ Figure 12d shows the XPS spectrum of the O 1s core level spectrum where the peak fitting shows a major component at 531.7 eV corresponding to the formation of metal oxides accompanied by 3 minor components at 529.5, 530.5 and 534.1 eV consistent with C-O and C=O species probably associated with organic contaminant loosely attached to the surface. This data is consistent with the galinstan surface being oxidized during the galvanic replacement process thereby giving up electrons for the reduction of gold ions to metallic gold and primarily forming Ga_2O_3 with contributions from In_2O_3 and SnO_2 due to the oxygenated aqueous environment under which the reaction is undertaken.

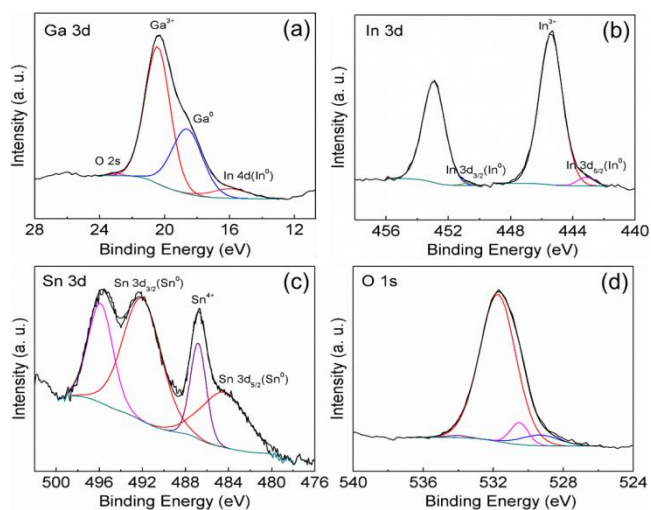


Figure 12. XPS spectra of Au-GaInSn nanocomposite. (a) Ga 3d, (b) In 3d, (c) Sn 3d and (d) O 1s core level spectra.

Metallic nanoparticles are well known for their catalytic activity towards electron charge transfer reactions. Recently we demonstrated the *in situ* formation of catalytically active materials from a galinstan precursor using NaBH_4 .⁴⁷ In order to explore the applicability of the colloidal Ag-GaInSn and Au-GaInSn materials we studied the degradation of MB using NaBH_4 in the presence of Ag and Au based nanocomposites. Therefore, colloidal solutions (0.1 ml) were added to MB and NaBH_4 solution mixtures in a cuvette and the progress of the reaction was monitored by UV-vis spectroscopy. The reduction of MB to leucomethylene blue could be monitored by measuring the intensity of the characteristic band at 664 nm associated with the oxidized form (MB^+) that gives rise to an intense blue colour in oxygenated environments.⁴⁹ As depicted in Figure 13a, in the case of Ag-GaInSn, the intensity of the peak at 664 nm was reduced by 80% in only 2 min. When Au-GaInSn was utilized the intensity of the peak decreased by 63% in 12 min (Figure 13b). Therefore, the Ag-GaInSn catalyst delivers better catalytic activity compared to Au-GaInSn which is evident by the larger reaction rate (0.805 min^{-1} vs. 0.084 min^{-1}). In a control experiment the catalysts were kept in $1.2 \times 10^{-2} \text{ M NaBH}_4$ for 180 min and subsequently studied by SEM and EDX. In the case of the Ag-GaInSn based catalyst, the morphology changed to micrometer sized spherical particles decorated with Ag nanoparticles during the course of contact with the reducing media. The composition also changed where the gallium concentration was significantly reduced (to ~3%), whereas the indium, tin and Ag elements were preserved with indium and tin maintaining a 2:1 ratio (Figure S6). In fact, gallium was dissolved to produce sodium gallate ($\text{NaGa}(\text{OH})_4$) as confirmed by EDX mapping (Figure S7). This is very similar to what we observed previously when galinstan was used as a catalyst for 4-Nitrophenol reduction using NaBH_4 .⁴⁷ In that case, when galinstan was brought into contact with sodium borohydride, gallium leached out of the liquid metal leaving behind a catalytically active solid In/Sn rich spherical micro/nanosized particles. Pure galinstan was also investigated for the MB reduction reaction, whereby a galinstan droplet sonicated in water was used as the catalyst. It was found that there was some catalytic activity (Figure S8) with a reaction rate of 0.011 min^{-1} , which is significantly

lower than that observed with Ag or Au present. Therefore, the Ag and Au nanomaterials facilitate the two electron transfer process between BH_4^- and MB^+ and increase the electron capacity of the catalyst. This behaviour is consistent with previous studies where Se nanowires decorated with Au nanoparticles showed increased activity for this reaction compared to only Se nanowires.⁵⁰ The observation in the current experiment confirms that, indeed, the enhanced catalytic activity of the material obtained from the Ag based nanocomposite could be due to a synergistic contribution of Ag and In/Sn rich particles. In contrast, when the Au-GaInSn based catalyst was treated with sodium borohydride, the nanorice morphology was not compromised and the Ga content was maintained in the sample (Figure S9). In addition, the presence of discrete Au nanoparticles could still be observed in the sample. In this system, it appears that the presence of Au rather than Ag stabilises Ga in the nanorice particles against leaching in the NaBH_4 solution. This observation may also explain the lower catalytic activity of the Au based catalyst as the presence of higher levels of gallium in galinstan based materials impairs catalytic activity for these types of reactions.

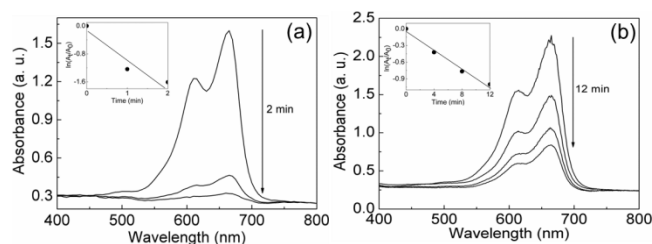


Figure 13. Time dependent UV-vis absorption spectra of the reduction of 7.2×10^{-5} M MB by an excess of NaBH_4 in the presence of (a) Ag-GaInSn and (b) Au-GaInSn based catalysts (insets: plots of $\ln(A_t/A_0)$ versus time).

CONCLUSION

In this work, we have demonstrated that the galvanic replacement of the liquid metal galinstan is possible via simple immersion in AgNO_3 or KAuBr_4 aqueous solutions. For large sized liquid metal droplets, the outer surface is converted into a solid Ag or Au rich material while the core remains liquid. The compositions and morphology of the outer metallic skin are determined by the precursor metal ion salt concentration. This process can be readily extended to other metals such as platinum, palladium and copper and illustrates how precious metal ions can be easily recovered from aqueous solution. At the micro/nanoscale micrometer sized droplets of galinstan created via sonication in the presence of AgNO_3 and KAuBr_4 resulted in the formation of Ag-GaInSn and Au-GaInSn nanorice particles as well as isolated Ag and Au nanoparticles. These materials were investigated for their catalytic activity for the reduction of methylene blue in the presence of NaBH_4 where it was found that the Ag-GaInSn material performed better due to the conversion of the catalyst into a Ag-In/Sn rich material. The work opens up a new approach to galvanic replacement and can be adopted to create many other combinations of liquid metal marbles or nanomaterials.

ASSOCIATED CONTENT

Supporting Information. EDX analysis of black silver formed in AgNO_3 aqueous solution of various concentrations, EDX analysis of black gold formed in KAuBr_4 aqueous solution of various concentrations, EDX analysis of the nanocomposite obtained via sonication in aqueous solution of various metal precursors, FESEM images of black gold formed on a galinstan droplet in 0.1 and 1 mM KAuCl_4 aqueous solution, EDX profile across the liquid metal core obtained after cutting through the black gold skin, EDX profile across nanostructures shown in high resolution SEM image obtained in 1 mM KAuBr_4 aqueous solution via sonication, FESEM image and EDX mapping of KInBr_3 , FESEM image of nanostructures obtained after adding 1 mM KAuBr_4 solution to galinstan already sonicated in DI water for 30 min, FESEM and EDX profile of Ag-GaInSn based catalyst created in 1.2×10^{-2} M NaBH_4 , FESEM image and EDX mapping of sodium gallate created from the treatment of Ag-GaInSn based catalyst in 1.2×10^{-2} M NaBH_4 , time dependent UV-vis absorption spectra of the reduction of 7.2×10^{-5} M MB by an excess of NaBH_4 in the presence of galinstan based catalyst, FESEM and EDX profile of Au-GaInSn based catalyst created in 1.2×10^{-2} M NaBH_4 . This material is available free of charge via the Internet at <http://pubs.acs.org>.

AUTHOR INFORMATION

Corresponding Author

* Email: anthony.omullane@qut.edu.au

Funding Sources

AOM gratefully acknowledges support from the Australian Research Council (Future Fellowship FT110100760).

ACKNOWLEDGMENT

The data reported in this paper were obtained at the *Central Analytical Research Facility* operated by the *Institute for Future Environments* (QUT). Access to CARF is supported by generous funding from the Science and Engineering Faculty (QUT).

REFERENCES

- Sun, Y.; Mayers, B. T.; Xia, Y. *Nano Lett.* **2002**, *2*, 481.
- Xia, X.; Wang, Y.; Ruditskiy, A.; Xia, Y. *Adv. Mater.* **2013**, *25*, 6313.
- Cobley, C. M.; Xia, Y. *Mater. Sc. Eng. R* **2010**, *70*, 44.
- Wang, X.; Feng, J.; Bai, Y.; Zhang, Q.; Yin, Y. *Chem. Rev.* **2016**, DOI: 10.1021/acs.chemrev.5b00731.
- Zhu, C.; Du, D.; Eychmüller, A.; Lin, Y. *Chem. Rev.* **2015**, *115*, 8896.
- Jones, M. R.; Osberg, K. D.; Macfarlane, R. J.; Langille, M. R.; Mirkin, C. A. *Chem Rev.* **2011**, *111*, 3736.
- Fang, Z.; Wang, Y.; Liu, C.; Chen, S.; Sang, W.; Wang, C.; Zeng, J. *Small* **2015**, *11*, 2593.
- Gilroy, K. D.; Farzinpour, P.; Sundar, A.; Hughes, R. A.; Neretina, S. *Chem. Mater.* **2014**, *26*, 3340.
- Niu, K.-Y.; Kulinich, S. A.; Yang, J.; Zhu, A. L.; Du, X.-W. *Chem. Eur. J.* **2012**, *18*, 4234.

10. Lu, X.; Chen, J.; Skrabalak, S. E.; Xia, Y. *Proc. Institution Mech. Eng., N: J. Nanoeng. Nanosystems* **2007**, *221*, 1.
11. Hu, S.; Tian, M.; Ribeiro, E. L.; Duscher, G.; Mukherjee, D. *J. Power Sources* **2016**, *306*, 413.
12. Liu, D.; Li, W.; Feng, X.; Zhang, Y. *Chem. Science* **2015**, *6*, 7015.
13. Jang, H.; Min, D.-H. *ACS Nano* **2015**, *9*, 2696.
14. Qin, X.; Liu, L.; Xu, A.; Wang, L.; Tan, Y.; Chen, C.; Xie, Q. *J. Phys. Chem. C* **2016**, *120*, 2855.
15. Sung, H. K.; Kim, Y. *Mater. Lett.* **2015**, *145*, 154.
16. Yin, Y.; Erdonmez, C.; Aloni, S.; Alivisatos, A. P. *J. Am. Chem. Soc.* **2006**, *128*, 12671.
17. Bansal, V.; Jani, H.; Du Plessis, J.; Coloe, P. J.; Bhargava, S. K. *Adv. Mater.* **2008**, *20*, 717.
18. Chen, J.; Glaus, C.; Laforest, R.; Zhang, Q.; Yang, M.; Gidding, M.; Welch, M. J.; Xia, Y. *Small* **2010**, *6*, 811.
19. Oh, M. H.; Yu, T.; Yu, S.-H.; Lim, B.; Ko, K.-T.; Willinger, M.-G.; Seo, D.-H.; Kim, B. H.; Cho, M. G.; Park, J.-H.; Kang, K.; Sung, Y.-E.; Pinna, N.; Hyeon, T. *Science* **2013**, *340*, 964.
20. Susman, M. D.; Popovitz-Biro, R.; Vaskevich, A.; Rubinstein, I. *Small* **2015**, *11*, 3942.
21. Pearson, A.; O'Mullane, A. P. *ChemPlusChem* **2013**, *78*, 1343.
22. Pearson, A.; O'Mullane, A. P.; Bansal, V.; Bhargava, S. K. *Inorg. Chem.* **2011**, *50*, 1705.
23. Pearson, A.; O'Mullane, A. P.; Bhargava, S. K.; Bansal, V. *Inorg. Chem.* **2012**, *51*, 8791.
24. Pearson, A.; Ramanathan, R.; O'Mullane, A. P.; Bansal, V. *Adv. Funct. Mater.* **2014**, *24*, 7570.
25. Blaber, M. G.; Engel, C. J.; Vivekchand, S. R. C.; Lubin, S. M.; Odom, T. W.; Schatz, G. C. *Nano Lett.* **2012**, *12*, 5275.
26. Vivekchand, S. R. C.; Engel, C. J.; Lubin, S. M.; Blaber, M. G.; Zhou, W.; Suh, J. Y.; Schatz, G. C.; Odom, T. W. *Nano Lett.* **2012**, *12*, 4324.
27. Tang, S.-Y.; Khoshmanesh, K.; Sivan, V.; Petersen, P.; O'Mullane, A. P.; Abbott, D.; Mitchell, A.; Kalantar-zadeh, K. *Proc. Nat. Acad. Sc.* **2014**, *111*, 3304.
28. Sivan, V.; Tang, S.-Y.; O'Mullane, A. P.; Petersen, P.; Kalantar-zadeh, K.; Khoshmanesh, K.; Mitchell, A. *Appl. Phys. Lett.* **2014**, *105*, 121607.
29. Hodes, M.; Rui, Z.; Lam, L. S.; Wilcoxon, R.; Lower, N. *Components, Packaging and Manufacturing Technology, IEEE Transactions* **2014**, *4*, 46.
30. So, J.-H.; Koo, H.-J.; Dickey, M. D.; Velev, O. D. *Adv. Funct. Mater.* **2012**, *22*, 625.
31. Li, G.; Wu, X.; Lee, D.-W. *Sens. Act. B* **2015**, *221*, 1114.
32. So, J.-H.; Thelen, J.; Qusba, A.; Hayes, G. J.; Lazzi, G.; Dickey, M. D. *Adv. Funct. Mater.* **2009**, *19*, 3632.
33. Boley, J. W.; White, E. L.; Kramer, R. K. *Adv. Mater.* **2015**, *27*, 2355.
34. Sheng, L.; Teo, S.; Liu, J. J. *Med. Biol. Eng.* **2016**, *36*, 265.
35. Koo, H.-J.; So, J.-H.; Dickey, M. D.; Velev, O. D. *Adv. Mater.* **2011**, *23*, 3559.
36. Dickey, M. D. *ACS Appl. Mater. Interf.* **2014**, *6*, 18369.
37. Sivan, V.; Tang, S.-Y.; O'Mullane, A. P.; Petersen, P.; Eshtiaghi, N.; Kalantar-zadeh, K.; Mitchell, A. *Adv. Funct. Mater.* **2013**, *23*, 144.
38. Zhang, W.; Ou, J. Z.; Tang, S.-Y.; Sivan, V.; Yao, D. D.; Latham, K.; Khoshmanesh, K.; Mitchell, A.; O'Mullane, A. P.; Kalantar-zadeh, K. *Adv. Funct. Mater.* **2014**, *24*, 3799.
39. Zhang, W.; Naidu, B. S.; Ou, J. Z.; O'Mullane, A. P.; Chrimes, A. F.; Carey, B. J.; Wang, Y.; Tang, S.-Y.; Sivan, V.; Mitchell, A.; Bhargava, S. K.; Kalantar-zadeh, K. *ACS Appl. Mater. Interf.* **2015**, *7*, 1943.
40. Arning, M. D.; Minter, S. D. In *Handbook of Electrochemistry*; Zoski, C. G., Ed.; Elsevier: Amsterdam, 2007.
41. Zhang, H.; Xu, J.-J.; Chen, H.-Y. *J. Phys. Chem. C* **2008**, *112*, 13886.
42. Plowman, B.; Ippolito, S. J.; Bansal, V.; Sabri, Y. M.; O'Mullane, A. P.; Bhargava, S. K. *Chem. Commun.* **2009**, 5039.
43. Zhang, X. G.; Li, X. H.; Li, H. L. *J. Colloid Inter. Sc.* **2001**, *234*, 68.
44. Ye, W.; Yan, J.; Ye, Q.; Zhou, F. *J. Phys. Chem. C* **2010**, *114*, 15617.
45. Hohman, J. N.; Kim, M.; Wadsworth, G. A.; Bednar, H. R.; Jiang, J.; LeThai, M. A.; Weiss, P. S. *Nano Lett.* **2011**, *11*, 5104.
46. Shafiei, M.; Motta, N.; Hoshyargar, F.; O'Mullane, A. P., In *SENSORS, 2015 IEEE* 2015, 1.
47. Hoshyargar, F.; Khan, H.; Kalantar-zadeh, K.; O'Mullane, A. P. *Chem. Commun.* **2015**, *51*, 14026.
48. Wiley, B.; Sun, Y.; Mayers, B.; Xia, Y. *Chem. Eur. J.* **2005**, *11*, 454.
49. Mowry, S.; Ogren, P. J. *J. Chem. Ed.* **1999**, *76*, 970.
50. Ray, C.; Dutta, S.; Sarkar, S.; Sahoo, R.; Roy, A.; Pal, T. *RSC Adv.* **2013**, *3*, 24313.

